Surface Enrichment in a Miscible Random Copolymer Blend: Influence of Polydispersity and Architecture

Robert Oslanec,[†] Jan Genzer,[‡] Alessandro Faldi,[§] and Russell J. Composto*

Department of Materials Science & Engineering and Laboratory for Research on the Structure of Matter, The University of Pennsylvania, Philadelphia, Pennsylvania 19104-6272

Paul D. Garrett

Solutia Inc., Springfield, Massachusetts 01151

Received April 17, 1998; Revised Manuscript Received February 3, 1999

ABSTRACT: Neutron reflectivity and low-energy forward-recoil spectrometry were used simultaneously to monitor surface segregation in blends of poly(styrene-*ran*-acrylonitrile), dSAN23 and SAN27, having 23 and 27 wt % AN, respectively. Because of its lower AN content, dSAN23 was found to partition at the polymer/air interface, in agreement with the work of Mansfield et al. (*Physica B* **1991**, *173*, 207) and Kim et al. (*Polymer* **1995**, *36*, 2427). In contrast to the previous studies, this work explores surface segregation at high dSAN23 bulk volume fractions, ϕ_∞ (i.e., $\phi_\infty > 0.50$). New results include the observation of a maximum dSAN23 surface excess (∼75 Å) near $\phi_\infty \approx 0.35$ and a dSAN23 surface volume fraction that approaches 1, rather than 0.75, as ϕ_∞ increases to 1. The dSAN23 profile deviates from the exponential profile predicted by Schmidt−Binder and self-consistent mean-field (SCMF) models. For $\phi_\infty > 0.50$, the profile displays a surface flattening not observed at low ϕ_∞. The SCMF model is extended to account for polymer polydispersity. Although thicker than the monodisperse profile, the polydisperse profile does not capture the experimentally detected surface flattening. Coil deformation along the surface is given as a possible explanation.

Introduction

The surface composition of a multicomponent blend plays an important role in many applications, including coatings, lubricants, or biomaterials, because it controls performance-related surface properties, such as adhesion, wetting, lubrication, or biocompatibility. In most cases, it is the lower surface energy component that enriches the blend surface. This surface enrichment can be further enhanced by increasing the typically unfavorable interaction between the components in the melt while maintaining a miscible mixture. Polymers are particularly sensitive to these driving forces, as compared to the small molecule systems. The connectivity of a large number of segments and the resulting small combinatorial entropy of mixing cause surface segregation even in systems in which the difference between the surface affinities of the components is very small. For example, a deuterated polymer has only a slightly smaller surface energy than that of its natural abundance counterpart. Yet it will surface-segregate from isotopic mixtures of sufficiently long macromolecules if the surface energy gain is greater than the demixing and gradient penalties associated with forming an enriched layer.

Surface segregation in isotopic blends has been studied extensively in the past.[1−10] Although the first quantitative segregation study in polymers focused on polystyrene (PS) and poly(vinyl methyl ether) (PVME) blends,[11] surface segregation studies of dissimilar polymers have received little attention. In particular, random copolymer blends (AB) containing different A contents represent model systems to explore surface enrichment because the surface and interaction energies can be tuned by continuously varying the copolymer composition. In a random copolymer blend of poly(ethylene-*ran*-ethyl ethylene) (dPE_xPEE_{1-x}), Steiner and co-workers[12] found that the copolymer with higher PEE content partitioned at the surface. Bruder and Brenn,[13] Gluckenbiehl et al.[14] and recently, Genzer et al.[15,16] investigated blends of deuterated polystyrene (dPS) and poly(styrene-*ran*-4-bromostyrene) (PBr_xS) in which x was the mole fraction of 4-bromostyrene. Having a lower surface energy than PBr_xS, dPS was found to partition at the air/mixture interface. Whereas monodisperse polymers are used in these and other studies, surface segregation experiments in blends having one or two polydisperse components are limited. Examples of the latter include PS/PVME,[11,17] PS/poly(ethylene oxide),[18] and poly(styrene-*ran*-acrylonitrile) (SAN) blends, dS_xAN_{1-x}/S_yAN_{1-y}, where $x \neq y$.[19,20] However, in these studies the influence of polydispersity on surface segregation was not explored. Because many industrially important blends contain polydisperse polymers, such as those made by free-radical polymerization, it is important to quantitatively explore the influence of polydispersity on the near surface volume fraction profile of polymer blends.

Poly(styrene-*ran*-acrylonitrile) is an engineering resin found in electronics, automotive, and medical applications. SAN is also widely used as the continuous phase in acrylonitrile−butadiene−styrene, a resin with excellent impact strength.[21] Regarding bulk thermodynamics, SAN blends are homogeneous if the AN difference is less than ∼5 wt %.[22] Using neutron reflectivity (NR) and dynamic secondary ion mass spectrometry (DSIMS),

* To whom correspondence should be addressed.
[†] Current address: BHP Institute for Steel Processing, University of Wollongong, Australia.
[‡] Current address: Department of Chemical Engineering, North Carolina State University, Raleigh, North Carolina 27695-7905.
[§] Current address: Exxon Chemical Company, P.O. Box 5200, 5200 Bayway Drive, Baytown, Texas 77522-5200.

10.1021/ma980601z CCC: $18.00
Published on Web 05/18/1999

Mansfield et. al.[19] studied surface segregation in miscible blends of dSAN23/SAN27 having acrylonitrile (AN) contents of 22.6 and 27.2 wt %, respectively. Kim and co-workers used conventional and time-of-flight forward-recoil spectrometry to probe the surface properties of the same blend.[20] In both studies, dSAN23 was found to segregate to the air/polymer interface. Moreover, the measured values of the dSAN23 surface excess, z^*, and the dSAN23 surface volume fraction, ϕ_1, from these two independent experiments are in good agreement with each other. In addition to surface segregation, dSAN23 was found to enrich the polymer/silicon interface.[19] As the dSAN23 bulk volume fraction, ϕ_∞, in the dSAN23/SAN27 mixtures increased from 0.025 to 0.20, z^* increased almost linearly with ϕ_∞ and then leveled off at $z^* \approx 75$ Å for $\phi_\infty \approx 0.35$. As ϕ_∞ increased, ϕ_1 increased rapidly at low ϕ_∞, slowed near $\phi_\infty \approx 0.1$, and then began to asymptotically approach $\phi_1 \approx 0.75$ near $\phi_\infty \approx 0.2$. Similar to previous surface segregation experiments, these studies are limited to measuring z^* and ϕ_1 at low values of ϕ_∞. An objective of this paper is to explore surface segregation over the broadest range of ϕ_∞ to date. In particular, our results show that the previous conclusions regarding the behavior of ϕ_1 versus ϕ_∞[20] were ambiguous. Our experiments demonstrate that as ϕ_∞ increases from 0.025 to 0.80, ϕ_1 increases more slowly between $\phi_\infty \approx 0.025$ and 0.2 and then continues to slowly approach 1 as ϕ_∞ approaches 1.

Theoretically, the equilibrium concentration profile near the surface can be established by balancing the free energy gain associated with placement of the lower surface energy component at the surface with the free energy penalty for creating a concentration gradient in the sample. Nakanishi and Pincus[23] and Schmidt and Binder (SB)[24] solved this problem using mean-field theory based on evaluating the analytical expressions for the free energy functional. Recently, Genzer and co-workers used a more accurate self-consistent mean-field (SCMF) model to describe surface segregation in binary polymer blends.[25] In particular, the values of z^* and ϕ_1 predicted by the SCMF model were in excellent agreement with those measured by Zhao et al. on isotopic blends of two high-molecular-weight polystyrenes,[6] whereas the SB model provided just a qualitative description of surface segregation in this system.

We have recently presented a comprehensive discussion concerning the applicability of both models.[15] We showed that although the SB model is capable of *qualitatively* describing surface segregation in polymer blends, the SCMF model, being more *quantitative*, should be the model of choice. In addition, because it treats only monodisperse polymers, the SB model cannot be used to describe surface segregation in a polydisperse system. On the other hand, the SCMF model can easily be modified to describe the surface segregation in polydisperse polymer systems. By the use of NR, the experimental profile is measured and found to deviate from the exponential-like functional form predicted by the SCMF model for monodisperse polymers. Rather, the profile follows a hyperbolic tangent form having a rounded shoulder near the surface and a thicker surface layer. These experimental profiles differ from those measured by Mansfield et al.[19] and Kim et al.[20] for the same system. One possible reason for this difference is that Mansfield et al. and Kim et al. studied blends having $\phi_\infty < 0.35$, whereas this study explores the behavior of mixtures at much larger bulk volume fractions, $\phi_\infty > 0.5$. Similar profile flattening in the near-surface region was observed for deuterated poly(ethylene propylene), (dPEP) segregating from dPEP/PEP blends at high dPEP concentrations.[10] Norton and co-workers attributed this behavior to the breakdown of mean-field theory. To determine if the polydispersity effect can describe our experimental results, the SCMF model presented by Genzer et al.[25] is extended to include the effect of molecular weight distribution for both species. Including the polymer polydispersity effects results in a more gradual decay in the near-surface volume fraction and a thicker profile away from the surface. However, the agreement between the experimental and polydisperse SCMF profiles is not significantly better than in the monodisperse case. The influence of copolymer architecture is given as a possible explanation.

Self-Consistent Mean-Field Model

Our implementation of the SCMF model follows the approach by Hong and Noolandi[26] and Shull.[27,28] Following the approach of Laub and Koberstein,[29] the polydispersity effect was accounted for by modifying the SCMF model for surface segregation of monodisperse polymers.[25] To start, the molar mass distribution curve[30] of polymer k is subdivided into a finite number, P, of fractions (typically $P = 10-20$). Each fraction is characterized by a degree of polymerization, $N_{k,n}$, and partial volume fraction, $\phi_{k,n}$. The partial volume fractions are normalized to satisfy

$$\sum_{n=1}^{p} \phi_{k,n} = \phi_k \tag{1}$$

where ϕ_k is the total volume fraction of polymer k. The Gibbs free energy density of mixing, G, is given by

$$\frac{G}{\rho_o k_B T} = \sum_{(k)} \sum_{n=1}^{p} \frac{\phi_{k,n} \ln \phi_{k,n}}{N_{k,n}} + \frac{1}{2} \sum_{j \neq k} \chi_{jk} \sum_{n=1}^{p} \phi_{j,n} \sum_{m=1}^{p} \phi_{k,m} \tag{2}$$

where k_B is Boltzmann's constant, T is the absolute temperature, ρ_0 is the monomer density, and χ_{jk} is the segmental interaction parameter between species j and k. The chemical potential, $\mu_{k,n}$, for fraction n of polymer k is given by[31]

$$\frac{\mu_{k,n}}{N_{k,n}} = \frac{\partial(G/\rho_o)}{\partial \phi_{k,n}} + \frac{G}{\rho_o} - \sum_{(k)} \phi_{k,n} \frac{\partial(G/\rho_o)}{\partial \phi_{k,n}} \tag{3}$$

In eq 3, the derivatives with respect to $\phi_{k,n}$ are taken at constant $\phi_{j,n}$ where $j \neq k$. The mean-field potential for each fraction in layer i is

$$w_{k,n}(i) = \frac{1}{N_{k,n}}[\mu_{k,n}(i) - \mu^0_{k,n}] - k_B T \frac{\ln \phi_{k,n}}{N_{k,n}} - \Delta w(i) - \Delta w_{ext}(1) \tag{4}$$

where $\mu^0_{k,n}$ is the chemical potential of the nth fraction of polymer k in the bulk, $\Delta w(i)$ is the incompressibility term, and $w_{ext}(1)$ is the external potential acting on polymer k. The incompressibility of the mixture is enforced by[27,28]

$$\Delta w(i) = k_B T\zeta[1 - \sum_{(k)}\sum_{n=1}^{p}\phi_{k,n}(i)] \quad (5)$$

where ζ is proportional to the bulk compressibility of the mixture. The influence of the surface on the polymers is introduced via the external field, $w_{ext}(1)$. We assume that the short-range forces dominate the interaction between the polymer and the surface; thus, only the polymer segments directly adjacent to the surface ($i = 1$) are under the influence of $w_{ext}(1)$.

The statistical description of a polymer chain enters the model via the segment probability distribution function, $q_k(i, j)$,[32] which represents the probability that the jth segment of polymer k is found on layer i. Functions $q_k(i, j)$ are found by solving the modified diffusion equation.[27,28] The choice of P, the number of polymer fractions of a polydisperse polymer, is very important. To obtain an accurate description of the molecular weight distribution, particularly at high polydispersities, P should be relatively large. On the other hand, to make the calculation computationally tractable, P should be small. We found that a good compromise can be achieved for $P = 10$. To further reduce computation time, the polymer volume fraction profiles are calculated for chain lengths that are smaller than the experimental values. The SCMF results are then rescaled as described later.

Experimental Section

Materials and Sample Preparation. Poly(styrene-*ran*-acrylonitrile) random copolymer with 27.2 wt % acrylonitrile (SAN27) was blended with deuterated SAN with 22.6 wt % AN (dSAN23). Only the styrene segments in dSAN23 were deuterated. The AN distribution was measured by HPLC at Solutia Inc. For both SAN27 and dSAN23, the distribution is Gaussian with a standard deviation of 2−2.5 wt %. As discussed later, this distribution was, however, neglected in SCMF calculations. Details of the SAN synthesis and characterization were given in Kim et al.[33] Table 1 summarizes the copolymer characteristics used in this study. A statistical segment length of $a = 6$ Å is used for both copolymers.[33] As a reference, the weight-average radius of gyration of dSAN23, $R_{g,dSAN23}$, is 110 Å.

The phase diagram of SAN27/dSAN23 depends on the molar masses and AN contents of each copolymer. ten Brinke et al.[34] and Cowie et al.[35] have shown that the Flory−Huggins interaction parameter for two random copolymers, χ_{blend}, is given by

$$\chi_{blend} = (x - y)^2\chi_{S-AN} \quad (6)$$

where χ_{S-AN} is the styrene−acrylonitrile interaction parameter, and x and y are the AN mole fractions in each copolymer. From previous measurements,[36] we calculate χ_{S-AN} and χ_{blend} to be 0.176 and 4.4×10^{-4}, respectively, at our experimental temperature, $T = 169$ °C. Although in the one-phase region, this blend has an interaction parameter that is very close to its critical value, $\chi_c = 8.34 \times 10^{-4}$.[37] In previous studies,[19,20] isotopic blends of SAN having the same AN content did not show any surface segregation. Thus, the dominant driving force for surface segregation is the difference in AN content, $x - y$. Furthermore, these studies provide supporting evidence for using $\chi_{S-AN} = \chi_{dS-AN}$ in eq 6.

For neutron reflectivity studies, the copolymers were dissolved in methyl isobutyl ketone and films of dSAN23/SAN27 blends were prepared by spin-coating the solutions on a silicon wafer (2 in. in diameter, 4.5 mm thick) previously etched for 3 min in a 7 vol % HF/water solution to remove the native silicon oxide layer. For ion-scattering experiments, thicker samples were prepared by spin-coating a more viscous solution having a higher dSAN23/SAN27 concentration on a silicon wafer. Samples were dried in a vacuum oven at 80 °C. The dSAN23 volume fractions and ellipsometric thicknesses are summarized in Table 2. The thin and thick films were chosen to optimize the sensitivity and resolution of neutron reflectivity and low-energy forward-recoil spectrometry (LE-FRES), respectively. These samples were annealed under vacuum ($\sim 10^{-4}$ Torr) at 169 °C for 69 h and 10 days for NR and LE-FRES studies, respectively. Based on previous studies,[20] these annealing times are sufficient to produce equilibrium profiles.

Table 1. SAN Copolymer Characteristics[a]

					AN content	
polymer ID	M_n	M_w	$\bar{N}_w$	Pd	wt %	molar %
DSAN23	81 500	179 000	2010	2.2	22.6	38
SAN27	81 300	242 000	2908	2.98	27.2	43

[a] Obtained from and characterized by Solutia Inc.

Table 2. dSAN23 Bulk Volume Fraction, ϕ_∞, and Ellipsometric Film Thickness, t, for NR (SAN1−SAN3) and LE-FRES (FSAN1−FSAN3) Samples

sample ID	ϕ_∞	t (Å)
SAN1	0.56	1035
SAN2	0.66	1068
SAN3	0.76	1035
FSAN1	0.56	4145
FSAN2	0.66	4122
FSAN3	0.76	3600

NR was used to determine the scattering length density profiles of samples SAN1−SAN3. These profiles allowed the volume fraction profiles of both polymers to be determined. LE-FRES was applied to measure the surface excess and the bulk volume fraction of dSAN23 in samples FSAN1−FSAN3.

Techniques. The NR measurements were performed on samples SAN1−SAN3 at the POSYII reflectometer of the intense pulsed neutron source (IPNS) at Argonne National Laboratory in Argonne, IL.[38] The principles of NR and its application to polymer science problems were reviewed by Russell.[39] Briefly, at POSYII, a neutron beam with a wavelength distribution of $\lambda = 5-12$ Å impinges at an incident angle, θ, ranging from 0.3° to 2.0°. The reflected intensity is measured as a function of the perpendicular component of neutron momentum, $k = (2\pi/\lambda)\sin\theta$. From this intensity, the total scattering length density profile ($^b/_V$) and, consequently, the polymer volume fraction profiles can be determined. Contrast is achieved by labeling one component (preferably the surface active species) with deuterium to increase its $^b/_V$. The main advantages of NR are its excellent depth resolution (~10 Å) and sensitivity to large gradients in the volume fraction profile. Thus, NR is an excellent tool to study surface segregation in polymer blends.

Because the polymer volume fraction profile is not directly measured, an indirect approach involving trial and error is usually employed to interpret reflectivity data. Using an initial guess for the $^b/_V$ profile, the reflectivity is calculated after convolution with the instrument resolution function.[39] Then, the calculated reflectivity curve is compared to the experimental one. On the basis of the difference, the $^b/_V$ profile is modified, and a new reflectivity curve is calculated. This procedure is repeated until the calculated and experimental reflectivity curve are in agreement. The scattering length density profile was calculated from the dSAN23 volume fraction profile, $\phi(x)$, using the individual scattering length densities $(^b/_V)_{dSAN23} = 5.3 \times 10^{-6}$ Å^{-2} and $(^b/_V)_{SAN27} = 1.54 \times 10^{-6}$ Å^{-2} determined from standards. The volume fraction profile was generated using a truncated hyperbolic tangent function described previously.[15]

The experimental setup at IPNS allows one to measure reflectivity over a limited range of k at a given angle of incidence. To cover a broader range of k, the NR measurements were taken at angles of $\theta = 0.45°$ and 0.9°. The resolution, dk/k, is a constant value for each angle. For both data sets, a semiautomatic fitting routine[40] was employed, in which the

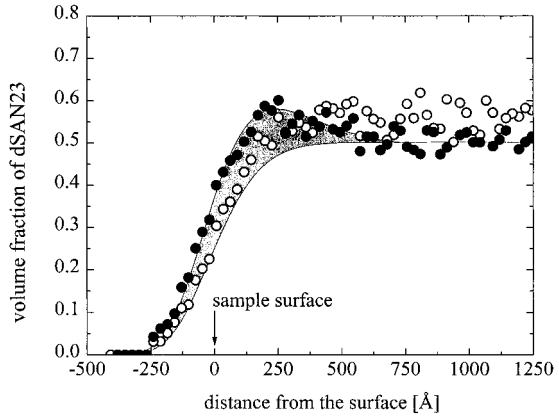

Figure 1. Volume fraction profiles of dSAN23 determined by LE-FRES for FSAN1 as-cast (open circles) and after annealing for 10 days at 169 °C (solid circles). The as-cast dSAN23 volume fraction is $\phi_\infty = 0.56$. The shaded area represents the dSAN23 surface excess, z^*, and the arrow indicates the position of the air/polymer interface.

shape of the volume fraction profile of deuterated polymer was varied at both the surface and the polymer/silicon interface (for more details see Genzer et al.[15]). In addition to the volume fraction profile, the thickness, the polymer/air and polymer/silicon roughness, and the instrumental resolution were varied. The reflectivity curve was calculated using a standard multilayer algorithm.[39,41] To determine the quality of the simulation, a standard χ^2 evaluation was used.[39] The volume fraction profiles used to fit the experimental data were practically identical for both angles, each having a different value of dk/k. The roughness at the polymer/substrate interface was determined from NR data collected from a standard (pure dSAN23), and very similar values were obtained from all other samples. Because the substrate preparation was identical for all samples, similar values of interface roughness are expected. One significant drawback of fitting NR data involves the question of profile uniqueness. This is particularly important if segregation occurs at two interfaces. To address this concern, a direct profiling technique was used to eliminate the ambiguity in fitting the NR data and to constrain the ranges of the fitting parameters in the NR analysis.

LE-FRES[42] was used to determine the concentration profile in samples FSAN1−FSAN3. In this version of LE-FRES, a 1.3 MeV beam of $^4He^+$ ions strikes the sample at a 15° glancing angle with respect to the surface. Inside the target, the $^4He^+$ ions collide with nuclei and recoil the lighter hydrogen (^1H) and deuterium (^2H) ions from the sample. To prevent the forward-scatter $^4He^+$ particles from masking the recoil signal, a 4.5 μm thick Mylar stopper foil is placed in front of the detector. Because recoiled ^1H and ^2H originating from beneath the surface are detected at lower energies than those of the corresponding surface nuclei, the energy spectrum provides a direct measure of the depth distribution of ^1H and ^2H. In addition, the yields of ^1H and ^2H are proportional to the volume fraction of the normal and deuterated polymers, respectively. Because the depth resolution is ≈400 Å, LE-FRES is incapable of resolving the exact shape of the volume fraction profiles. However, LE-FRES has the sensitivity to directly measure the surface excess and bulk volume fraction down to 5 Å and 0.01, respectively.[42] LE-FRES thus represents an excellent complementary tool to the higher resolution but indirect NR technique.

Results

We have studied surface segregation in random copolymer blends of dSAN23 and SAN27 having 22.6 and 27.2 wt % AN, respectively. Because of the small difference in AN content, dSAN23 and SAN27 are miscible.[22] Figure 1 shows the dSAN23 volume fraction profile in the near-surface region of sample FSAN1, as measured by LE-FRES. The position of the air/polymer interface is marked by an arrow in Figure 1. The dSAN23 volume fraction in the as-cast sample (open circles) is homogeneous, $\phi_\infty = 0.56$, indicating that dSAN23 does not segregate to the surface during spin-coating. Upon annealing at 169 °C for 10 days, the surface becomes enriched with dSAN23 (closed circles), the lower surface energy component. The surface excess of dSAN23, $z^* = 66$ Å, is represented by the shaded area in Figure 1. One reason for the lack of experiments at high values of ϕ_∞ is the large background-to-signal (z^*) ratio (cf. Figure 1). Notice that to conserve dSAN23, the dSAN23 bulk volume fraction decreases to $\phi_\infty' \approx 0.5$ to compensate for the dSAN23 driven to the surface region. The values of ϕ_∞, ϕ_∞', and z^* for FSAN1−FSAN3 are summarized in Table 3. By combining these results at high ϕ_∞' with previous ones at low ϕ_∞', we can more accurately describe the behavior of z^* versus ϕ_∞'.

Table 3. LE-FRES Results

sample ID	ϕ_∞[a]	ϕ_∞'[b]	z^* (Å)
FSAN1	0.56	0.502	66.0
FSAN2	0.66	0.617	57.3
FSAN3	0.76	0.728	34.0

[a] Bulk volume fraction in as-cast sample. [b] Bulk volume fraction in annealed sample.

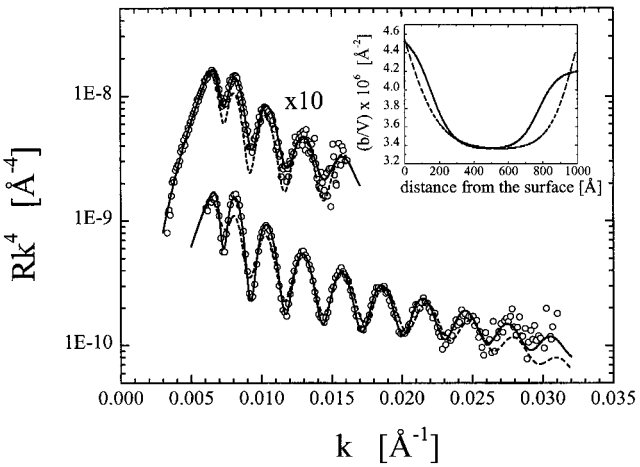

Figure 2. Neutron reflectivity data (open circles) of the SAN1 sample after annealing for 69 h at 169 °C. The top ($\theta = 0.45°$) and bottom ($\theta = 0.9°$) curves are shifted for clarity. The solid and dashed lines are the reflectivity simulations calculated from the $^b/_V$ flattened and exponential profiles, respectively, shown in the inset.

Figure 2 shows the neutron reflectivity spectrum of SAN1 after annealing at 169 °C for 69 h. This sample has the same ϕ_∞ as FSAN1. The upper and lower curves correspond to $\theta = 0.45°$ and $\theta = 0.9°$, respectively. The solid lines represent best fits to the reflectivity curves calculated using the scattering length density profile shown by the solid line in the inset to Figure 2. The sample thickness of 1004 Å obtained from the fitting is in very good agreement with ellipsometry results (cf. Table 2). The good agreement between the measured and simulated spectra is reflected in the low χ^2 values of 1.4 and 3.6 at low and high angles, respectively. As apparent from the $^b/_V$ profile, the higher $^b/_V$ component, dSAN23, strongly segregates to both the air/polymer and polymer/silicon interfaces. As mentioned earlier, the segregation at both interfaces was also observed by Mansfield[19] using DSIMS on blends with $\phi_\infty \leq 0.21$. Figure 2 also shows reflectivity curves simulated using profiles in which the $^b/_V$ decay was exponential (dashed

Table 4. NR Results

sample ID	ϕ_∞[a]	ϕ_∞' [b]	ϕ_1	z^* (Å)
SAN1	0.56	0.485	0.792	51.9
SAN2	0.66	0.615	0.836	49.5
SAN3	0.76	0.723	0.876	28.6

[a] Bulk volume fraction in as-cast sample. [b] Bulk volume fraction in annealed sample.

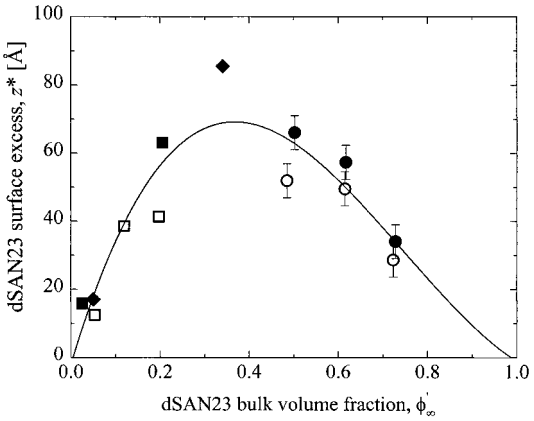

Figure 3. Surface excess of dSAN23, z^*, as a function of dSAN23 bulk volume fraction, ϕ_∞'. Solid circles represent LE-FRES values whereas open circles are from NR. The error bars were obtained by a standard procedure.[43] Also shown are the z^*'s measured by Mansfield et al.[19] using NR (open squares) and DSIMS (solid squares) and by Kim et al.[20] using TOF−FRES (solid diamonds). The solid line is a guide to the eye.

curves). The best fit to the experimental data was obtained using the $^b/_V$ profile shown by the dashed curve in the inset. Relative to the flattened profile, the exponential profile resulted in poorer agreement between the measured and simulated spectra. Quantitatively, the χ^2 parameter increased by ca. 10x at low and high angles (i.e, 19.2 and 25.3, respectively).

From the $^b/_V$ profiles (e.g., inset to Figure 2), the dSAN23 volume fraction profiles are evaluated for SAN1−SAN3. Table 4 summarizes the surface segregation characteristics, namely ϕ_∞', z^*, and the dSAN23 volume fraction at the surface, ϕ_1. As ϕ_∞' increases, z^* decreases by nearly 45%, whereas ϕ_1 only increases by about 10%. The dependence of z^* and ϕ_1 on dSAN23 concentration will be presented next.

By combining these new results ($\phi_\infty' > 0.5$) with previous studies ($\phi_\infty' < 0.5$),[19,20] a comprehensive picture of surface segregation in dSAN23/SAN27 blends can be assembled. In Figure 3, the dSAN23 z^*'s found in this paper and by Mansfield et al.[19] and Kim et al.[20] are shown. Figure 3 shows that z^* initially increases rapidly as ϕ_∞' increases, reaches a maximum value of about 75 Å near $\phi_\infty' = 0.35$, and then more slowly decreases again toward zero as ϕ_∞' approaches 1. Initially, the increase in z^* is driven by the gain in surface energy associated with replacing SAN27 segments located at the surface by dSAN23 segments. Near $\phi_\infty' = 0.35$, z^* reaches a maximum because the entropic penalty for demixing limits further segregation of dSAN23 chains to the surface. For $\phi_\infty' > 0.35$, this entropic penalty acts to decrease z^* relative to its maximum value.

Figure 4 shows that ϕ_1 increases rapidly as ϕ_∞' increases from 0 to 0.20. However, ϕ_1 increases more slowly beyond $\phi_\infty' \approx 0.3-0.4$. This transition in ϕ_1 versus ϕ_∞' is observed over the same ϕ_∞' range at which z^* reaches its maximum value (cf. Figure 3). Subsequently, ϕ_1 asymptotically reaches 1 as ϕ_∞' approaches 1. Initially, ϕ_1 increases rapidly because of the lower dSAN23 surface energy relative to SAN27. Similar to the behavior of z^*, further increases in ϕ_1 are retarded by the entropy penalty associated with demixing. For $\phi_\infty' > 0.4$, ϕ_1 asymptotically approaches 1 as the bulk becomes pure dSAN23. This latter observation contradicts the ϕ_1 versus ϕ_∞ behavior reported in Kim et al.[20] Over a limited range of ϕ_∞ (0.05 to 0.20), Kim et al.[20] report that ϕ_1 apparently saturates at a value of 0.75 near $\phi_\infty \approx 0.20$. This example points out the inherent problems with extrapolating surface segregation measurements at low ϕ_∞ to predict the behavior of ϕ_1 (and z^*) at high ϕ_∞.

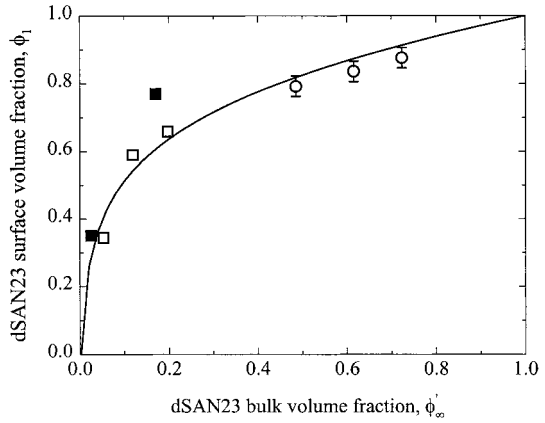

Figure 4. Surface volume fraction of dSAN23, ϕ_1, as a function of the dSAN23 bulk volume fraction, ϕ_∞'. Open circles represent values obtained from NR and have error bars determined by a standard procedure.[43] Also shown are values of ϕ_1 measured by Mansfield et al.[19] using NR (open squares) and DSIMS (solid squares). The solid line is a guide to the eye.

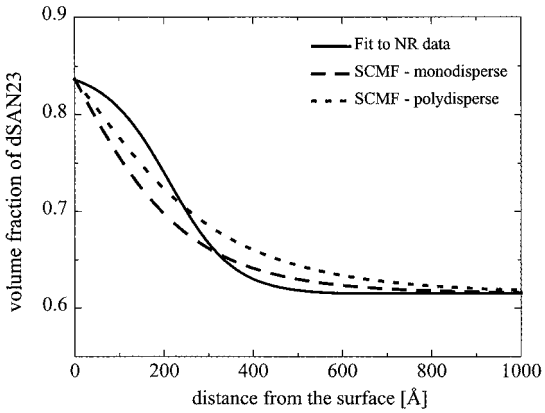

Figure 5. Volume fraction profiles of dSAN23 in SAN2 obtained from NR (solid line) calculated using the monodisperse SCMF (dashed line) and polydisperse SCMF (dotted line) models. Note that only the near-surface region is shown. The SCMF parameters are given in the text.

Discussion

For SAN1−SAN3, the volume fraction profiles are determined in the high ϕ_∞ regime using neutron reflectivity. Figure 5 shows the dSAN23 volume fraction profile in SAN2 (solid line) annealed at 169 °C for 69 h. The dSAN23 surface excess and surface volume fraction are 49.5 Å and 0.836, respectively. Defined as the distance between the sample surface (=0) and the profile inflection point, the thickness of the segregated layer is quite large, about 2 times $R_{g,dSAN23}$. In contrast to the low ϕ_∞ studies, the volume fraction profile near the

surface is flat. As discussed below, the profile itself decreases more gradually than the exponential decay predicted by the SB or SCMF models. To test the sensitivity to profile shape, the NR fitting was repeated with an exponential profile (cf. Figure 2). However, the best exponential fits were in poor agreement with the experimental results. Quantitatively, the χ^2 values for exponential fits were almost an order of magnitude greater than the χ^2 for the tanh profile in Figure 5. Note that at low ϕ_∞ previous experiments on the same system did uncover a flat profile near the surface, although an exponential profile was used in the data analysis.[19] Similar surface flattening was reported for surface segregation of dPEP from dPEP/PEP.[10] Norton and coworkers found that as the ϕ_∞ of dPEP decreases from 0.149 to 0.053, the surface flattening becomes less pronounced. A similar tendency is observed in dSAN23/SAN27. Namely, the flattening of the profiles is most pronounced at the highest ϕ_∞ (SAN3), decreases as ϕ_∞ decreases (SAN2 and SAN1), and disappears for lower values of ϕ_∞.[19] Surface flattening has also been observed in dPS/PS blends at large ϕ_∞ using DSIMS[6] and NR.[3] The broadening in this homopolymer blend, however, was much smaller than that in the random copolymer SAN blend. In recent studies using nuclear reaction analysis to depth profile dPS/PS, Zink et al.[44] find that the dPS profile is in good agreement with the SB prediction and that surface flattening is not observed within the resolution limit (110 Å fwhm). These conflicting results point out the need for further detailed experiments such as those presented here.

Because of the SB limitations discussed previously,[15,25] a SCMF model is used to calculate the dSAN23 volume fraction profile. In the initial model, dSAN23 and SAN27 are assumed to be monodisperse with weight average degrees of polymerization of 2010 and 2908, respectively. In Figure 5, the monodisperse model is shown as the dashed line using $\chi_{blend} = 4.4 \times 10^{-4}$, $\phi_\infty' = 0.615$, and $a = 6$ Å. In the SCMF calculation, the value of the excess surface free energy, $-dF_s/d\phi_1$, is systematically varied until the SCMF and NR values of ϕ_1 are equal. By the use of this method, the $-dF_s/d\phi_1$ for SAN2 is found to be 0.05 Å, in agreement with values by Kim et al.[20] The values of $-dF_s/d\phi_1$ for SAN1 and SAN3 are the same, 0.05 ± 0.01 Å. Note that the magnitude of $-dF_s/d\phi_1$ is about 3 times larger than that in dPS/PS[1,3,6,8,25] and similar to values reported for dPEP/PEP[10] and dPS/PBr$_{0.049}$S.[15]

The experimental and monodisperse SCMF profiles differ significantly, however. As shown in Figure 5, the SCMF profile (dashed line) follows an exponential shape and fails to display the surface flattening found in the experimental profile. Correspondingly, the SCMF profile underestimates the experimental profile in the near-surface region, resulting in a smaller z^*, 43.2 Å, compared to the experimental value, 49.5 Å. Similar differences in z^* were also found for the SAN1 and SAN3 systems using $-dF_s/d\phi_1 = 0.05$ Å. Recently, Jones[45] and Genzer et al.[25] included long-range interactions in the SB and SCMF models, respectively, and found that they had only a minor effect on the profiles. Thus, surface flattening is not likely to be due to long-range interactions. By including the influence of surface confinement on local chain correlations, Freed[46] has suggested a possible molecular level explanation for surface flattening.

Table 5. Scaling Parameters for SCMF Calculations

	original parameters			scaled parameters			
polymer ID	$\bar{N}_w$	$\bar{N}_n$	a (Å)	$\bar{N}_w'$	$\bar{N}_n'$	a' (Å)	Pd index
DSAN23	2010	915	6	223	102	18	2.2
SAN27	2908	977	6	323	109	18	2.98

To provide a more accurate description, the SCMF model is modified to include the polydispersity of dSAN23 and SAN27, where Pd = 2.2 and 2.98, respectively. Each copolymer is divided into 10 fractions of monodisperse chains having different segment numbers. The volume fractions of these 10 fractions are described by a Schulz molar mass distribution.[30] Because of the long chain lengths and large number of copolymer fractions, the computation time to solve the SCMF equations is unreasonable given the computing resources available. To reduce this time, the number of segments and segment lengths are rescaled while holding R_g and polymer density constant. The statistical segment length (and lattice spacing) increases from 6 Å to $a' = 18$ Å. Correspondingly, the number of segments decreases by a factor of 9. The chain parameters used in the polydisperse SCMF model are shown in Table 5.

For the SAN2 blend, the dSAN23 volume fraction profile calculated from the polydisperse SCMF model is represented by the dotted line in Figure 5. The parameters used in this calculation include $\chi_{blend} = 4.4 \times 10^{-4}$, $\phi_\infty' = 0.615$, and those listed in Table 5. As in the monodisperse model, $-dF_s/d\phi_1$ was systematically varied until the SCMF and NR values of ϕ_1 agreed. For the polydisperse SCMF model, $-dF_s/d\phi_1 = 0.06 \pm 0.01$ Å for SAN1−SAN3, similar to the $-dF_s/d\phi_1$ found in the monodisperse SCMF model. Figure 5 shows that the polydisperse profile is thicker and decays more gradually than the monodisperse profile, resulting in a z^* (=57.2 Å) that is larger than the experimental value (49.5 Å). The profile of the polydisperse blend is thicker, in part, because of the high molar mass fraction of dSAN23 now included in the model. However, the polydisperse model fails to reproduce the flattening of the near-surface region observed in the experimental profile. As in the monodisperse case, the polydisperse profile follows an exponential shape. These results indicate that the flattening observed in the dSAN23 volume fraction profile is likely not caused by the molecular weight polydispersity of SAN. As mentioned before, the AN content polydispersity, about 2−2.5 wt % for SAN27 and dSAN23, was neglected in our SCMF models. This small variation in AN content, however, is not expected to change the statistical nature of SAN copolymers. Recently, Gersape et al.[47] calculated the volume fraction profiles of end-tethered copolymer chains using Monte Carlo and lattice SCMF models. Although random and alternating copolymers had volume fraction profiles flatter than that of a block copolymer with the same composition, the difference between random and alternating copolymer volume fraction profiles was negligible. Thus, a small change in the randomness of the AN distribution in the copolymer should not significantly influence the volume fraction profile. The AN content polydispersity can, however, affect the surface energies of both SAN copolymers and consequently their surface behavior. This effect deserves further investigation.

In addition to the AN content polydispersity, we have also considered the effect of copolymer chain end groups.

Unfortunately, the chemical nature of the chain ends is unknown. We, know, however,[33] that both copolymers were synthesized in a similar way and therefore have similar chain ends. The effect of chain ends on the polymer surface properties was examined by Jalbert et al.[48] on a series of end-functionalized poly(dimethysiloxane) polymers. The authors reported that the surface tension of end-functionalized polymer chains was given by a combination of surface tensions of end groups and repeat segments. For long polymer chains, however, the contribution of chain ends was negligible. On the basis of the analysis of Jalbert et al., the end groups contribute only 0.1% and 0.07% to the total surface tension of dSAN23 ($N \approx 2000$) and SAN27 ($N \approx 3000$), respectively. As mentioned, we assume that the chain ends are similar in both polymers, and therefore, there is a negligible surface energy difference between the chain ends of dSAN23 and SAN27.

As shown by the experimental profile in Figure 5, the flat region thickness extends into the bulk by about $^1/_3\xi - ^1/_2\xi$, where ξ is the bulk correlation length of dSAN23/SAN27.[37] Note that this flat region is smaller than $R_{g,dSAN23}$. For SAN1 and SAN3, the surface flattening has a similar thickness. Moreover, the flat region thickness is greater than the distance over which long-range forces can influence the profile shape.[25,45] A similar extent of profile flattening was observed by Norton et al. in dPEP/PEP blends,[10] and detected in Monte Carlo calculations by Rouault et al.[49] This range of surface flattening indicates that correlations smaller than R_g or ξ are important. Such correlations are, however, ignored in the SB and SCMF models which are based on mean-field theory. Thus, a nonmean-field theory that accounts for correlations between the chains near the surface may more accurately describe these results.

Rouault and co-workers performed Monte Carlo calculations for small chains with 32 segments and indeed found profile flattening with a thickness of $^1/_3\xi - ^1/_2\xi$.[49] The authors attribute the flattening to chain connectivity and the chain's resistance against elastic deformation. As a result, the instantaneous shape of a Gaussian polymer coil is a "soap-shaped" object defined by three gyration eigenvectors. Because the eigenvector directions are randomly oriented in space, on average, the polymer coil is spherically symmetric in the bulk. However, the situation is different when a polymer coil is placed near an interface, such as a free surface. Here, optimum packing is achieved by slightly deforming the coil such that the longest, R_g^{max}, and shortest, R_g^{min}, eigenvectors are parallel and perpendicular to the surface, respectively. Thus the elastically deformed polymer coil of thickness $\sim R_g^{min}$ lies flat on the surface plane and occupies approximately $(R_g^{max})^2$ of surface area. Within that coil, the polymer volume fraction is nearly constant. In this framework, the closest distance that a nonsegregating chain can approach the surface is $\sim R_g^{min}$; hence, the profile within R_g^{min} of the surface should be relatively flat. Naturally this flattening becomes more pronounced as the surface concentration of coils increases, in qualitative agreement with our experimental results. Although both the free surface and the polymer/substrate interfaces are effectively impenetrable, the polymer chains at the free surface have more freedom to relax than chains in contact with the substrate. Thus the profile flattening is expected to be more pronounced at the polymer/substrate interface as indeed demonstrated in the inset of Figure 2.

The magnitude of R_g^{min} is governed by the polymer−surface interaction strength, intrachain interactions, and chain architecture. As noted, the excess surface free energy for dSAN23/SAN27 is comparable with that of dPEP/PEP and dPS/$PBr_{0.048}$S blends and approximately 3 times larger than that of dPS/PS. The segment−segment interactions χ are strongly repulsive for the SAN blend, $\chi_{S-AN} = 0.176$ at 169 °C, whereas in the other blends the χ parameter is much lower: for example, $\chi_{dPS/PBrS} \approx 0.07$ at 170 °C.[13−15] For the isotopic blends, χ is even smaller, on the order of 10^{-4} for dPEP/PEP at 70 °C,[10] and $\approx 1.7 \times 10^{-4}$ for dPS/PS at 170 °C.[50] Therefore, the SAN coil is considerably more resistant against compression and deformation, which in turn results in higher values of R_g^{min}. Finally, the third crucial parameter is the chain architecture. Random copolymers consisting of dissimilar repulsive segments will have a greater resistance against deformation than, for example, homopolymers in which all segments along the chain are equal. In addition, steric hindrance will also tend to increase R_g^{min}. In this light, the flattening of the surface region of dSAN23 volume fraction profiles at high ϕ_∞ can be qualitatively understood if the random copolymer nature of the chain is taken into account along with the highly positive S−AN interaction parameter. To support this interpretation, however, more rigorous models including the influence of local correlations and chain architecture are needed.

Conclusion

In this paper, we described the surface segregation behavior of dSAN23 from miscible blends of dSAN23 and SAN27. Using LE-FRES, we have measured the dSAN23 surface excess, z^*, for $\phi_\infty > 0.5$. The volume fraction profiles of dSAN23 near the surface were measured using NR. From these studies, the surface volume fraction of dSAN23, ϕ_1, as a function of ϕ_∞' was extracted. In combination with previous studies limited to low values of ϕ_∞' (<0.35), we have provided for the first time a complete description of surface segregation behavior of SAN blends. We have found that z^* has its maximum value near $\phi_\infty' \approx 0.35$. Correspondingly, ϕ_1 initially increases rapidly with ϕ_∞' and then more slowly for $\phi_\infty' > 0.35$.

The LE-FRES experiments were complemented by NR measurements of the dSAN23 volume fraction profiles. One unique feature of the profile is surface flattening. Similar flattening was observed in dPEP/PEP blends by Norton et al.[10] In contrast, no flattening was observed in blends of dSAN23/SAN27 at low values of ϕ_∞.[19,20] A monodisperse SCMF model underestimates z^* and predicts an exponentially decaying profile without surface flattening. Although a polydisperse SCMF model produces a thicker surface layer, the profile shape in the near-surface region is still exponential. On the basis of Monte Carlo simulations by Rouault et al.[49] we speculate that the profile flattening is closely related to local correlations and architecture of the polymer chain, which are governed by segment−segment interactions, chain stiffness, and the steric interaction between segments. To completely understand the origin of surface flattening, a nonmean-field model is needed that accounts for both the local chain correlations and chain architecture.

Acknowledgment. This research was supported by the National Science Foundation, Division of Materials

Science, under Grant No. DMR95-26357. The ion-scattering experiments and SCMF calculations made use of MRSEC Shared Experimental Facilities supported by the National Science Foundation under Grant No. DMR96-32598. Neutron reflectivity experiments were performed at the IPNS at Argonne National Laboratory, funded by Department of Energy, BES-MS, under Grant W-31-109-Eng-38. We thank Dr. Todd Mansfield for providing unpublished data and useful discussions, Dr. Wan C. Wu for synthesis of dSAN23 and SAN27, and Dr. Robert A. Mendelson for helpful suggestions. We also thank Roger C. Ayotte of Solutia Inc. for the molecular weight and AN distribution analysis.

References and Notes

(1) Jones, R. A. L.; Kramer, E. J.; Rafailovich, M. H.; Sokolov, J.; Schwarz, S. A. *Phys. Rev. Lett.* **1989**, *62*, 280.
(2) Jones, R. A. L.; Kramer, E. J. *Philos. Mag. B* **1990**, *62*, 129.
(3) Jones, R. A. L.; Norton, L. J.; Kramer, E. J.; Composto, R. J.; Stein, R. S.; Russell, T. P.; Mansour, A.; Karim, A.; Felcher, G. P.; Rafailovich, M. H.; Sokolov, J.; Zhao, X.; Schwarz, S. A. *Europhys. Lett.* **1990**, *12*, 41.
(4) Composto, R. J.; Stein, R. S.; Kramer, E. J.; Jones, R. A. L.; Mansour, A.; Karim, A.; Felcher, G. P. *Physica B* **1989**, *156−157*, 434. Composto, R. J.; Stein, R. S.; Felcher, G. P.; Mansour, A.; Karim, A. *Mater. Res. Soc. Symp. Proc.* **1990**, *166*, 485.
(5) Sokolov, J.; Rafailovich, M. H.; Jones, R. A. L.; Kramer, E. J. *Appl. Phys. Lett.* **1989**, *54*, 590.
(6) Zhao, X.; Zhao, W.; Sokolov, J.; Rafailovich, M. H.; Schwarz, S. A.; Wilkens, B. J.; Jones, R. A. L.; Kramer, E. J. *Macromolecules* **1991**, *24*, 5991.
(7) Hariharan, A.; Kumar, S. K.; Russell, T. P. *J. Chem. Phys.* **1993**, *98*, 4163. Hariharan, A.; Kumar, S. K.; Rafailovich, M. H.; Sokolov, J.; Zheng, X.; Duong, D.; Schwarz, S. A.; Russell, T. P. *J. Chem. Phys.* **1993**, *99*, 656.
(8) Budkowski, A.; Steiner, U.; Klein, J. *J. Chem. Phys.* **1992**, *97*, 5229.
(9) Hopkinson, I.; Kiff, F. T.; Richards, R. W.; Affrossman, S.; Hartshore, H.; Pethrick, R. A.; Munro, H.; Webster, J. R. P. *Macromolecules* **1995**, *28*, 627.
(10) Norton, L. J.; Kramer, E. J.; Bates, F. S.; Gehlsen, M. D.; Jones, R. A. L.; Karim, A.; Felcher, G. P.; Kleb, R. *Macromolecules* **1995**, *28*, 8621.
(11) Bhatia, Q. S.; Pan, D. H.; Koberstein, J. T. *Macromolecules* **1988**, *21*, 2166.
(12) Steiner, U.; Eiser, E.; Budkowski, A.; Fetters, L. J.; Klein, J. *Ber. Bunsen-Ges. Phys. Chem.* **1994**, *98*, 366. Schelfold, F.; Eiser, E.; Budkowski, A.; Steiner, U.; Klein, J.; Fetters, L. J. *J. Chem. Phys.* **1996**, *104*, 8786; **1996**, *104*, 8795. Budkowski, A.; Schelfold, F.; Klein, J.; Fetters, L. J. *J. Chem. Phys.* **1997**, *106*, 719.
(13) Bruder, F.; Brenn, R. *Europhys. Lett.* **1993**, *22*, 707.
(14) Gluckenbiehl, B.; Stamm, M.; Springer, T. *Colloids Surf. A* **1994**, *86*, 311.
(15) Genzer, J.; Faldi, A.; Oslanec, R.; Composto, R. J. *Macromolecules* **1996**, *29*, 5438.
(16) Genzer, J.; Composto, R. J. *Europhys. Lett.* **1997**, *38*, 171.
(17) Cowie, J. M. G.; Devlin, B. G.; McEwen, I. J. *Macromolecules* **1993**, *26*, 5628.
(18) Sakellariou, P. *Polymer* **1993**, *34*, 3408.
(19) Mansfield, T. L.; Composto, R. J.; Stein, R. S.; Rafailovich, M. H.; Sokolov, J.; Schwarz, S. A. *Physica B* **1991**, *173*, 207.
(20) Kim, E.; Kramer, E. J.; Garrett, P. D.; Mendelson, R. A.; Wu, W. C. *Polymer* **1995**, *36*, 2427.
(21) Kaplan, W. A., Ed. *Modern Plastics Encyclopedia*; McGraw-Hill: New York, 1996; 73.
(22) Molau, G. E. *Polym. Lett.* **1965**, *3*, 1007.
(23) Nakanishi, H.; Pincus, P. *J. Chem. Phys.* **1983**, *79*, 997.
(24) Schmidt, I.; Binder, K. *J. Phys. II (Paris)* **1985**, *46*, 1631.
(25) Genzer, J.; Faldi, A.; Composto, R. J. *Phys. Rev. E* **1994**, *50*, 2373 and references therein.
(26) Hong, K. M.; Noolandi, J. *Macromolecules* **1981**, *14*, 727.
(27) Shull, K. R.; Kramer, E. J. *Macromolecules* **1990**, *23*, 4769.
(28) Shull, K. R. *J. Chem. Phys.* **1991**, *94*, 5723; *Macromolecules* **1992**, *25*, 2122; **1993**, *26*, 2346.
(29) Laub, C. F.; Koberstein, J. T. *Macromolecules* **1994**, *27*, 5016.
(30) Schulz, G. V. *Z. Phys. Chem., Abt. B* **1939**, *43*, 25. Flory, P. J. *Principles of Polymer Chemistry*; Cornell University Press: Ithaca, NY, 1953.
(31) Sanchez, I. C. *Encycl. Polym. Sci. Technol.* **1987**, *11*, 1.
(32) Helfand, E.; Tagami, Y. *Polym. Lett.* **1971**, *9*, 741; *J. Chem. Phys.* **1972**, *56*, 3592; *57*, 1812.
(33) Kim, E.; Kramer, E. J.; Garrett, P. D.; Mendelson, R. A.; Wu, W. C. *J. Mater. Sci.* **1995**, *30*, 1709.
(34) ten Brinke, G.; Karasz, F. E.; MacKnight, W. J. *Macromolecules* **1983**, *16*, 1827.
(35) Cowie, J. M. G.; Lath, D. *Makromol. Chem., Macromol. Symp.* **1988**, *16*, 103.
(36) Higashida, N.; Kressler, J.; Yukioka, S.; Inoue, T. *Macromolecules* **1992**, *25*, 5259. Higashida, N.; Kressler, J.; Inoue, T. *Polymer* **1995**, *36*, 2761.
(37) de Gennes, P. G. *Scaling Concepts in Polymer Physics*; Cornell University Press: Ithaca, NY, 1979.
(38) Felcher, G. P.; Hilleke, R. O.; Crawford, R. K.; Haumann, J.; Kleb, R.; Ostrowski, G. *Rev. Sci. Instrum.* **1987**, *58*, 609.
(39) Russell, T. P. *Mater. Sci. Rep.* **1990**, *5*, 171.
(40) Genzer, J.; Oslanec, R., unpublished results.
(41) Born, M.; Wolf, E. *Principles of Optics*, 6th ed.; Pergamon Press: Oxford, 1980.
(42) Genzer, J.; Rothman, J. B.; Composto, R. J. *Nucl. Instrum. Methods* **1994**, *B86*, 345.
(43) Results were obtained by minimizing the χ^2 between experimental and simulated data. The error bars correspond to a factor of 2 increase in χ^2.
(44) Zink, F.; Kerle, T.; Klein, J. *Macromolecules* **1998**, *31*, 417.
(45) Jones, R. A. L. *Phys. Rev. E* **1993**, *47*, 1437.
(46) Freed, K. F. *J. Chem. Phys.* **1996**, *105*, 10572.
(47) Gersape, D.; Fasolka, M.; Israels, R.; Balazs, A. C. *Macromolecules* **1995**, *28*, 4758.
(48) Jalbert, C.; Koberstein, J. T.; Hariharan, A.; Kumar, S. K. *Macromolecules* **1997**, *30*, 4481.
(49) Rouault, Y.; Dünweg, B.; Baschnagel, J.; Binder, K. *Polymer* **1996**, *37*, 297.
(50) Bates, F. S.; Wignall, G. D.; Koehler, W. C. *Phys. Rev. Lett.* **1985**, *55*, 2425. Bates, F. S.; Wignall, G. D. *Phys. Rev. Lett.* **1986**, *57*, 1429.

MA980601Z